



The effect of diatom content on the physical, electrical, and mechanical properties of soils

Jeongki Lee¹ · Dante Fratta² · Angelica M. Palomino³

Received: 24 March 2022 / Accepted: 22 July 2023 / Published online: 20 September 2023
© The Author(s), under exclusive licence to Springer-Verlag GmbH Germany, part of Springer Nature 2023

Abstract

Biological-formed fossilized diatom sediments have unique physical, electrical, and mechanical properties due to the shape, internal open porosity, and brittleness of the individual particles. The presence of diatoms strongly influences the overall behavior of soils. However, engineers and researchers find this influence challenging to quantify because measuring fossilized diatom content is elusive. This paper uses simple physical, electromagnetic, and mechanical engineering measurements to characterize the response of the artificial soils prepared with known amounts of fossilized diatoms under different pore-chemistry fluid and mechanical environments. Soils with high fossilized diatom content tend to retain high quantities of water even under high NaCl-concentration pore fluid. This response results from the internal porosity and is not a function of electrical forces on the particle surface. Furthermore, internal porosity governs electrical and mechanical properties under different pore fluid environments. Despite having elevated Liquid Limits, soils with high fossilized diatoms content do not deform while drying and changing pore fluid salt concentration. However, fossilized diatoms are brittle and offer high compressibility and low particle crushing stress (around 2–4 MPa). Our results show that simple physical and index tests can help assess the effect of fossilized diatoms' in soils, and provide a framework to predict the engineering properties of natural soils containing a wide range of fossilized diatoms even when diatom content cannot be precisely measured.

Keywords Compression index · Dielectric permittivity · Diatomaceous earth · Dual porosity · Electrical conductivity · Fall cone · Fossilized diatom · Mercury intrusion · Particle crushing stress · Shrinkage limit

1 Introduction

Fossilized diatoms are the amorphous silicate exoskeleton of plankton and algae. Due to their hollow and angular tooth-like outer surface and flat circular or cylindrical shapes (Fig. 1a), diatoms have high friction angles (between 32° and 43°—[31, 111], and an open hollow structure (with intra-particle porosity as high as 60–70%—[65]). These properties make fossilized diatoms unique among most mineral soil particles. In addition, the intra-particle porosity allows diatomaceous earth to store large amounts of water in natural environments (up to 460%—[19, 31]). The water trapping ability and high friction angle of fossilized diatoms yield high Liquid Limits (100 to 550%) and Plasticity Indices (30 to 500%) [31, 60, 101, 111]. Despite its ability to retain high amounts of water, diatomaceous earth shows volumetric stability when drying, as most water is stored inside the particles [82]. So, while the high

✉ Dante Fratta
fratta@wisc.edu

Jeongki Lee
lee545@wisc.edu

Angelica M. Palomino
angel@utk.edu

¹ Smart Infra-Structure Technology Institute, Pukyong National University, Busan, South Korea

² Geological Engineering, Civil and Environmental Engineering, University of Wisconsin-Madison, Madison, WI, USA

³ Civil and Environmental Engineering, University of Tennessee, Knoxville, TN, USA

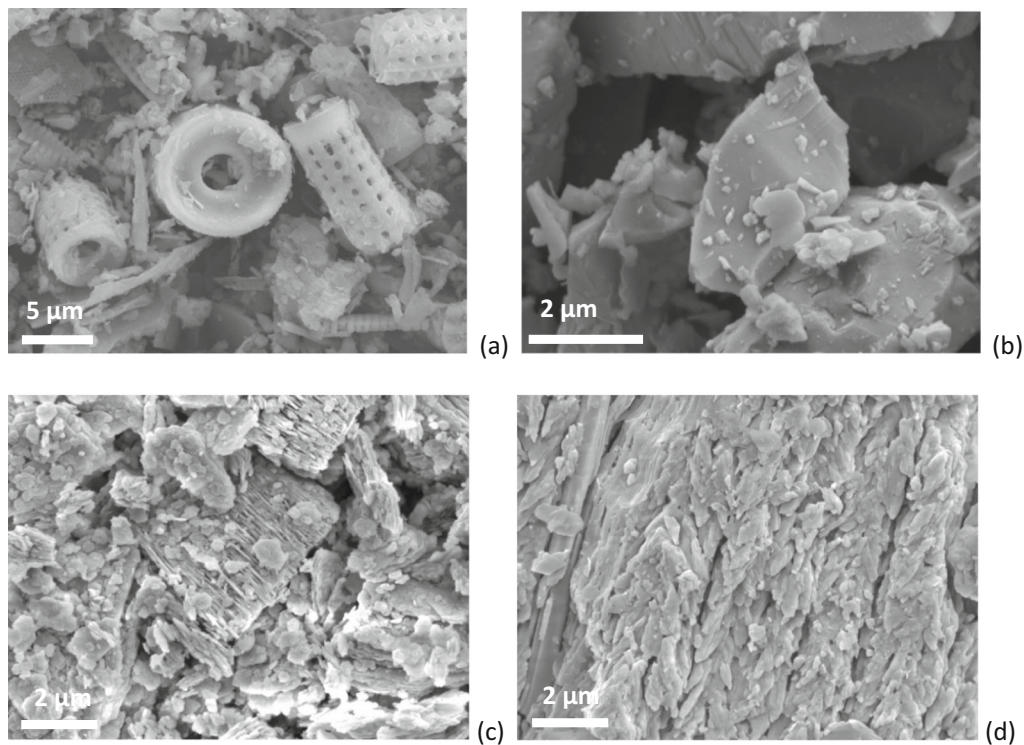


Fig. 1 Scanning Electron Microscope (SEM) images of tested fine-grained soils: **a** diatomaceous earth, **b** silica flour, **c** kaolinite, and **d** montmorillonite

friction angle and the volumetric stability hint at coarse-grained behavior, the high-water content and plasticity hint at fine-grained behavior of diatomaceous earth. To further confound the interpretation of diatomaceous earth behavior, Day [28] and Hong et al. [47] report compression indices of diatomaceous earth similar to those of fine-grained soils at low effective stresses. However, diatomaceous earth shows volumetric collapse when the fossilized diatoms crush at low effective stresses (in the low MPa range). In addition, the hydraulic conductivity of diatomaceous earth is higher than soils with similar porosity, Atterberg limits, and specific surface areas [97].

Other researchers have also observed atypical responses in soils containing fossilized diatoms. For example, Bryant and Rack [18] and MacKillop et al. [68] documented that sediment layers with high fossilized diatom content tend to have higher over-consolidation stresses and porosity than deposits immediately above or below them. Furthermore, fossilized diatom deposits have low erosion potential [66, 69, 105], and good slope resistance [97] due to their high friction angle and low unit weight. Nevertheless, while diatomaceous earth tends to be susceptible to dynamic liquefaction [35], clayey soils with greater than 50% diatom content show an increase in the static and cyclic resistance at stresses lower than 600 kPa [111].

To properly quantify the diatoms' contribution to soils' behavior, researchers tried to estimate the fossilized diatom

content in natural soils. Several methods are available: counting fossil particles from sediment samples [85], infrared absorption [26], X-ray diffraction [36], chemical analysis paired with a normative calculation [62], Teflon digestion bomb [33], and a variety of wet-chemical leaches [29, 34, 75, 76]. However, all these tests have limitations and accuracy problems, preventing their application in geotechnical engineering research and practice as they do not typically follow empirical correlations [28, 30, 68, 73, 97]. Researchers also tried to assess the differential characteristics of diatomaceous earth by sampling natural specimens or creating artificial ones. For example, researchers conducted tests to determine physical properties (i.e., particle size distributions, density, viscosity), index properties (i.e., Atterberg Limits), mechanical properties (compressibility, shear strength), and electrical properties [20, 21, 46, 80, 84, 113] by combining various fine soils and fossilized diatoms under more diverse conditions. Finally, Zuluaga-Astudillo et al. [115] just published a review of the state of art on the engineering behavior of diatomaceous earth. In their paper, they argued the importance of developing a new framework for assessing and classifying diatomaceous earth.

Despite their complex geotechnical properties, fossilized diatoms are applied in several industrial solutions (Table 1). For example, fossilized diatoms are used to remove bacteria and solids in water filters

Table 1 Engineering and scientific applications of diatoms and diatomaceous earth

Engineering/science areas	Application	References
Hydrogeology	Groundwater detoxification; desiccant aid	[86, 106]
Filtration	Filtration medium; dye removal from aqueous solution	[22, 103]
Water treatment	Microbial bioreactor for wastewater treatment; drinking water filtration; radioactivity removal from liquid waste	[88, 40, 79]
Geotechnical and Transportation Engineering	Filler in asphalt pavement; soil stabilization	[54, 72]
Structural Engineering	Cement reinforcement; concrete additive	[39, 53, 13, 114, 109]
Construction	Additive brick production for thermal insulators	[37]
Biology	Bacterium and solid impurity filter	[57]
Pesticides	Detoxification from aerial pesticide; reduction of risk synthetic pesticide residual exposure; pest control	[87, 1, 27]
Composites	Fillers in reinforced rubber (elastomer); plastic reinforcement as friction-resistant material	[70, 64]
Energy	Battery production; Solar cells	[71, 50]

Table 2 Basic properties of tested samples

Physical property	Diatomaceous earth	Silica flour	Kaolinite	Montmorillonite
Color	Seashell	White	Floral white	Linen
Specific gravity, G_s^a	2.24	2.61	2.57	2.65
Specific surface, S_s (m^2/g) ^b	102.5	1.5	26.5	400–800 ^g
Particle size, d_{50} (μm) ^c	8.3 ^h	13	2.4	0.8
Liquid Limit (%) ^d	130	30	53	300
Plasticity Index (%) ^e	30	5	27	255
pH (10% solids) ^f	7.47	8.2	5.46	-

^aASTM D5550 [11]—Specific gravity with helium gas

^bEthylene glycol monomethyl ether results by Akin and Likos [1] after Cerato and Lutenegeger[24]

^cASTM D7928 [10]—H type hydrometer

^dFall cone testing with Humboldt penetrometer for the Liquid Limit Test

^eASTM D4318 [5]—Standard method for the Plastic Limit Test

^fMeasured by using Thermo Scientific, Orion 5 Star

^gReported results from Santamarina et al.[94]

^hThe mean particle sizes were determined by modifying the interpretation of the ASTM D7928 standard [10]. During the analysis of the hydrometer test, the specific gravity of the silica in diatoms was reduced to compensate for the internal porosity of the particles (assumed to be 70%). A detailed analysis is presented by Miklasz and Denny [73]

[22, 40, 57, 79, 86, 88, 103, 106]. In addition, soil stabilization, asphalt and plastic filler, concrete additives, friction-resistant matrices, and thermal insulation have all benefited from fossilized diatoms' lightweight, hollow structure and shape [13, 37, 39, 53, 54, 64, 70, 72, 114]. Fossilized diatoms are also used for pest control as they dehydrate insects [1, 27, 87]. In addition, there are attempts to apply fossilized diatoms in energy fields to improve the discharge capacity of positive electrodes [50, 71].

Given the difficulties in determining fossilized diatom content in natural soils, the purpose of this study is to provide a framework to better predict the engineering

properties of natural soils containing a wide range of fossilized diatoms. In this study, we measured and documented the response of artificial mixtures of diatomaceous earth with three different fine-grained soils (i.e., silica flour, kaolinite, and montmorillonite). We used the results to identify how fossilized diatoms affect sediment behavior by targeting and comparing physical, electrical, and mechanical responses of particles with similar mineral composition but different particles shapes (including the presence of internal porosity—i.e., silica flour vs. fossilized diatoms), particles with similar particle sizes but different cation exchange capacities (i.e., kaolinite and

Table 3 Specimen conditions for each experiment

Test	Fine-grained soils	Mixture ratios	Pore fluid	Specimen condition	Test reference / standard
Sedimentation test	Diatomaceous earth, montmorillonite	100%:0%, 75%:25%, 50%:50%, 25%:75%, 0%:100%	Deionized water, and 0.01, 0.1, 1 M NaCl solutions	Saturated	[41, 82]
Electromagnetic characterization test	Diatomaceous earth, silica flour, kaolinite	100%:0%, 67%:33%, 33%:67%, 0%:100%	Air, deionized water	Dry, Unsaturated, Saturated	[8, 38, 93]
1D Oedometer Tests		100%:0%, 67%:33%, 33%:67%, 0%:100%	Deionized water	Saturated	[9]
Mercury intrusion test		100% diatomaceous earth	Mercury	Saturated	[6]
Atterberg Limits test	Diatomaceous earth, silica flour, kaolinite, montmorillonite	100%:0%, 50%:50%, 0%:100%	Deionized water, and 0.04, 1 M NaCl solutions	Saturated	[112, 5, 7]
Abrasion test		100% diatoms, 100% silica flour, 100% kaolinite, 100% montmorillonite	Air	Dry	[3]

montmorillonite vs. fossilized diatoms), and particles with different specific surface areas (i.e., silica flour, kaolinite and montmorillonite vs. fossilized diatoms). In addition, we evaluated how diatoms and mixtures respond to changes in pore fluid environments, high-stress conditions, and abrasion. These tests were employed to create differential responses for assessing the effect of diatom content in natural soils with low-cost and straightforward methodologies.

2 Materials

Mixtures of diatomaceous earth, silica flour, kaolinite, and montmorillonite soils were selected to include soils formed by particles of different sizes, shapes, mineralogies, specific surface areas, and surface charge densities. These mixtures provide a significant range in physical (i.e., Atterberg Limits and sedimentation), electromagnetic (i.e., electrical conductivity and dielectric permittivity), and mechanical (i.e., compression and abrasion responses) properties.

The source of freshwater diatomaceous earth was PREMA-GUARD, Inc. The particles have mostly centric (i.e., disk-type) and pennate (i.e., cylindrical) shapes [84, 115] with diameters ranging from 5 to 30 μm , lengths ranging from 10 μm to 50 μm , and internal openings ranging from 0.2 to 0.5 μm (Fig. 1a). Silica flour and diatoms have similar chemical compositions but without internal particle porosity. Premier Silica Inc. was the source of the tested silica flour. The silica flour passed the

No. 325 sieve (44 μm opening—Fig. 1b). Kaolinite consists of successive 1:1 layers of gibbsite-silica sheets, and strong hydrogen bonds attach these sheet layers. As a result, the kaolinite has relatively low swell potential and Atterberg Limits. The tested kaolinite was purchased from Old Hickory Clay Company (Fig. 1c). Finally, 2:1 layers of silica-gibbsite-silica sheets form the montmorillonite clays. Cations and van der Waals forces weakly bonded the sheets. As a result, montmorillonite clays have high swell potential and Atterberg Limits (Fig. 1d). The physical properties of the soils used in this study are documented in Table 2.

3 Methods

We used ASTM standards and other testing methodologies to assess the contribution of diatoms to physical, electrical, and mechanical properties. Table 3 summarizes all the tests performed and the type of material and fluid environments used. We did not test all material combinations in each testing methodology as we aimed to target different phenomena and mechanisms described in the following sections.

3.1 Electromagnetic wave characterization

Electromagnetic (EM) waves capture the interaction and percolation of different volumetric phases in soils [92, 102, 107]. The EM properties of the specimens—electrical conductivity and dielectric permittivity—were

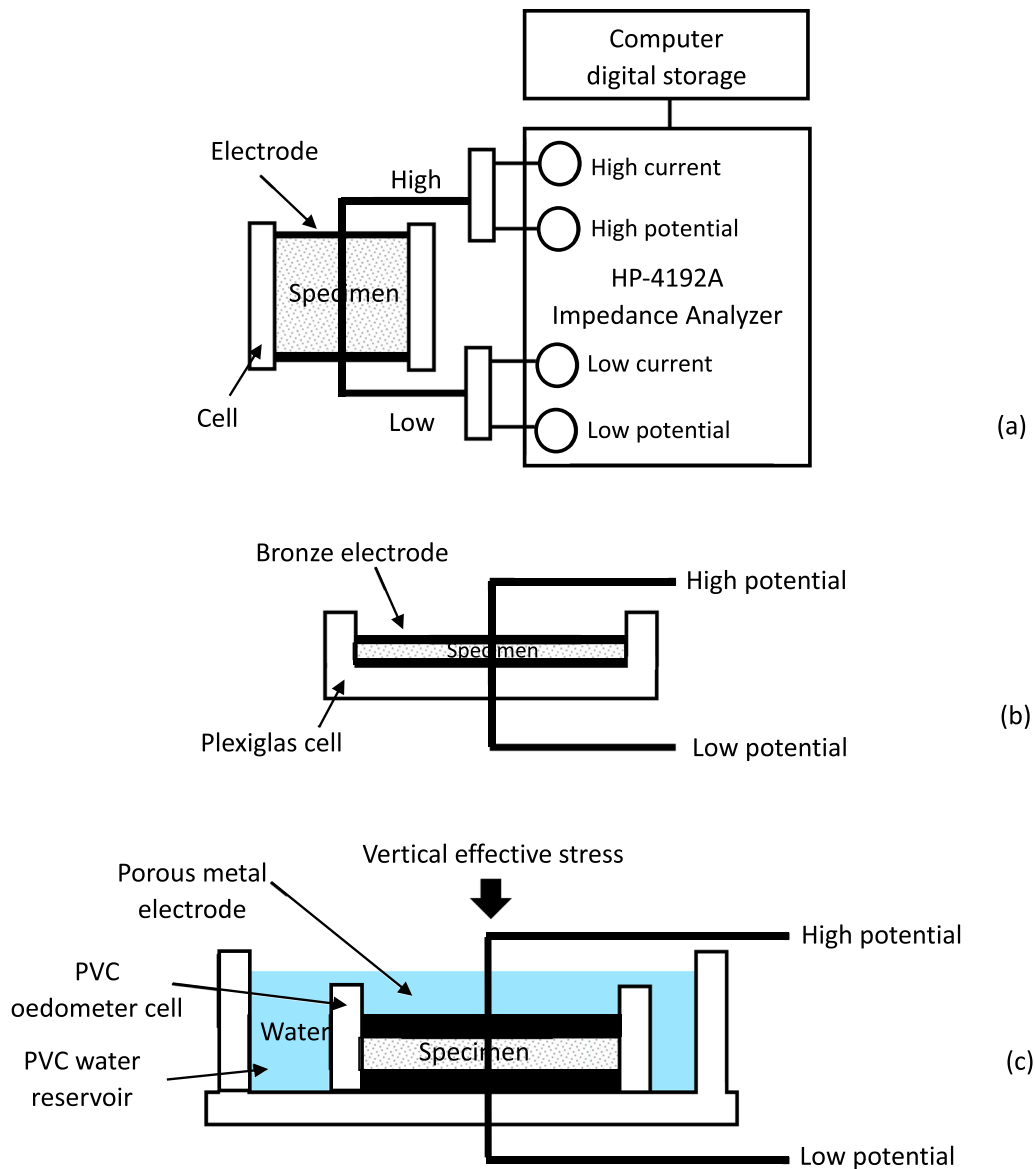


Fig. 2 Setup for dielectric permittivity and electrical conductivity measurements. **a** Test configuration and electronic peripherals. **b** Cell for dry specimens (diameter $d = 62.8$ mm and height $h = 4$ mm specimen), and **c** cell for saturated specimens ($d = 62.8$ mm and $h = 10$ mm)

measured as a function of diatom content, water content, and void ratio (as the effective stresses increase). We conducted these tests to evaluate the EM response of fine-grained soils and how the presence of diatoms influences these responses.

Soil specimens were tested with an HP 4192A Impedance Analyzer and the two-terminal electrode configuration (Fig. 2a). We used frequencies higher than 100 kHz to reduce electrode polarization effects, as Santamarina and Fratta [93] recommended. At the same time, we used small thickness/diameter ratios to minimize fringe effects [8, 38]. Finally, we converted the measured impedance values into real and imaginary components of the dielectric permittivity and electrical conductivity [38, 93, 94].

3.2 Sedimentation behavior of fine-grained soil

The way fine-grained particles settle and aggregate is a function of the particles' size and the fluid's chemical properties [28, 67, 96]. Furthermore, the sedimentation fabric captures the effect of pore fluid, temperature, and pressure during formation [99, 100]. Therefore, we tested mixtures at 100:0, 75:25, 50:50, 25:75, and 0:100 ratios of montmorillonite-diatomaceous earth ratios under different pore fluids. The pore fluids included deionized water, 0.01 M, 0.1 M, and 1 M of NaCl solutions mixed with 2% by volume of fine-grained soils [41, 82]. These tests complemented earlier results of Palomino et al. [82] with kaolin-diatoms mixtures.

3.3 Atterberg limits

Fine-grained soils gradually increase their volume when the water content increases and the consistency transitions from solid to semi-solid, plastic, and liquid. Shrinkage Limit, Plastic Limit, and Liquid Limit capture these transitions [77, 89, 110]. We used the Fall Cone Test (80-g mass with a 30° steel cone—[108, 112] to determine the undrained shear strength as an alternative to the Casagrande cup’s Liquid Limit measurements. In the Fall Cone Test, the Liquid Limit is the water content corresponding to an undrained shear stress of 1.7 kPa. The water content that yields an undrained shear strength of 170 kPa defines the Plastic Limit [43]. We also measured the Shrinkage Limit (i.e., a measure of the water content at which a fine-grained soil volume starts increasing) to establish the volumetric stability of different soils and the effect of the internal porosity in the diatoms. We followed the procedure described in the ASTM D4943 standard [7] with the modification to allow for different NaCl concentrations to help evaluate the sensitivity of the tested soils under different chemical environments.

3.4 Abrasion and confined compression tests

The Los Angeles Test assesses the abrasion resistance of aggregate materials. Particles degrade by grinding as the material tumbles in a 711-mm diameter and 508-mm long hollow steel drum rotating at 30 to 33 rpm filled with twelve 48-mm diameter steel balls (ASTM C131 [3]). The Los Angeles Tests ran for 1, 4, 12, and 24 h on pure samples of dry diatomaceous earth, silica flour, kaolinite, and montmorillonite. After each testing time, we measured Atterberg Limits and grain size distribution and took scanning electron microscope (SEM) images to assess their abrasion responses.

Finally, we evaluated particle crushing using oedometer tests (ASTM D2435 [4] with modified specimen dimensions) while monitoring how the stress–strain behavior changes with diatom content [23, 45, 59, 61]. We tested dry mixtures of 0%, 33%, 67%, and 100% diatomaceous earth with kaolinite and silica flour with vertical stress ranging from 100 kPa to 8 MPa. We aim to assess the contribution of diatoms on particle crushing. Mercury Intrusion Tests [6] captured the pore size distribution changes with increasing compression stresses.

4 Test results and interpretation

4.1 Permittivity properties

The properties and distribution of solid and fluid phases affect soils’ permittivity. Mixture models represent the contribution of the different phases in particulate media [52, 92, 95]:

$$\epsilon_m^\beta = (1 - n) \cdot \epsilon_p^\beta + \theta_v \cdot \epsilon_l^\beta + (n - \theta_v) \cdot \epsilon_g^\beta \tag{1}$$

where ϵ_i^β is the relative dielectric permittivity of the mixture (m), solid particles (p), liquid (l) and gas (g), n is the porosity, $\theta_v (= n \cdot S_r)$ is the volumetric water content, and S_r is the degree of saturation. The characteristic mixing factor β is a function of these phases’ relative interactions and arrangement to the direction of the applied electric field. When the layering is aligned parallel to the direction of the electric field, the characteristic mixing factor β is close to 1; when the layering is perpendicular to the direction of the electric field, the β becomes -1 ; and β is 0.5 for isotropic two-phase media [25, 52, 92]. For common natural soils,

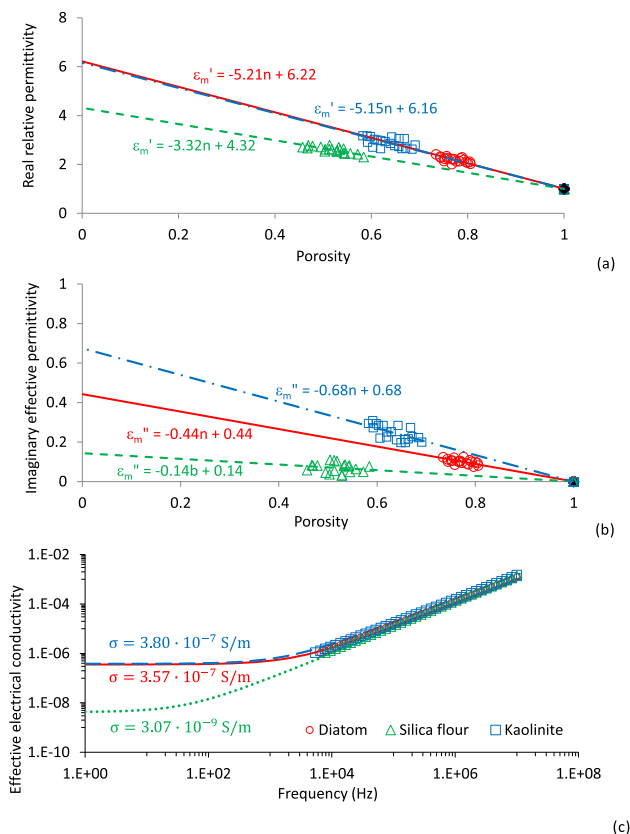


Fig. 3 Electromagnetic measurements of dried fine-grained soils: **a** real relative permittivity, **b** imaginary effective permittivity at 10 MHz as a function of porosity, and **c** effective electrical conductivity as a function of frequency for oven-dry fine-grained soils

the characteristic mixing factor β varies between 0.3 and 0.6.

Figure 3a, b shows the relative real and imaginary effective permittivity at 10 MHz as porosity increases. When the soil is dry, the effect of the interaction between multiple phases disappears with the absence of water (i.e., $\beta = 1$ in Eq. 1), and the response becomes a simple linear combination of the contribution of the volumetric phases. So, the solid particles' real and imaginary effective permittivity can be determined when the measurements extrapolate to zero porosity. The 10-MHz relative dielectric permittivity for the diatom particles is $\varepsilon_m^* = 6.22 - j \cdot 0.44$, for silica flour particles is $\varepsilon_m^* = 4.32 - j \cdot 0.14$, and for kaolinite particles is $\varepsilon_m^* = 6.16 - j \cdot 0.68$. We expected that diatoms and silica flour particles would have yielded similar values (within the range of the reported real relative permittivity for silica—between 3.6 and 4.5—[14, 48]). Either the biological origin of the diatoms or, most likely, the water still entrapped within the internal porosity of diatoms contributes to the greater estimated real and imaginary dielectric permittivity [63]. The imaginary permittivity is highest in kaolinite and the lowest in silica flour (Fig. 3b). The imaginary effective relative permittivity includes the effect of surface conduction, which should be most significant for kaolinite, even at low water contents [78, 90, 94]. We also estimated the effective electrical conductivity of diatomaceous earth $\sigma = 3.57 \cdot 10^{-7}$ S/m, silica flour $\sigma = 3.07 \cdot 10^{-7}$ S/m, and kaolinite $\sigma = 3.80 \cdot 10^{-7}$ S/m (Fig. 3c). Again and as expected, these values are slightly higher for kaolinite.

Figure 4 documents the increase of real relative permittivity as a function of volumetric water content at 10 MHz. The characteristic mixing factor β was estimated by fitting Eq. 1 to the data in Fig. 4. We used the real relative permittivity estimated for the different solid phases (Fig. 3a). A value of the parameter β close to 1 indicates that the particle arrangement is parallel to the electric field (i.e., low orientational polarization is favored). In contrast, $\beta = 0.5$ indicates an isotropic structure (Fig. 4a). The kaolinite and silica flour yield $\beta = 0.53$ and $\beta = 0.32$ (Fig. 4c, d), respectively; these values are within the range reported for natural soils (0.3 to 0.6). Results show that diatomaceous earth's parameter $\beta = 0.82$ is consistent with a lower orientational polarization (Fig. 4a, b). In addition, the dielectric permittivity does not increase smoothly with increasing volumetric water content in all three soils (Fig. 4b–d). Changes in the slope of the curves indicate transitions from unsaturated to saturated conditions at volumetric water contents of $\theta_v = 0.49$ for silica flour, $\theta_v = 0.51$ for kaolinite, and $\theta_v = 0.70$ for diatomaceous earth. The internal porosity of diatoms explains the greater volumetric water content in diatomaceous earth. Finally, Fig. 4e documents the complex interaction between

electrical conductivity and volumetric water content in the three tested soils. As the volumetric water content increases after reaching full saturation, the deionized water displaces the solid phase, surface conduction decreases, and low conduction of the liquid phases reduces the overall conductivity of the soils [12, 55, 91].

The real and imaginary relative effective permittivities in saturated mixtures change with decreasing volumetric water content as the effective vertical stress increases from 100 to 600 kPa (Fig. 5). Higher diatom contents yield increasing permittivity values because diatoms allow for high water contents (i.e., water permittivity is higher than other phases in the mixtures). However, mixes with kaolinite show greater orientational polarization and surface conductance than silica flour [94]. So, the real and imaginary permittivities are higher in kaolinite mixtures than in other mixtures at the same volumetric water content. Conversely, the permittivity difference between kaolinite and silica flour mixtures decreases with increasing diatom content.

4.2 Sedimentation tests

Sedimentation tests indirectly assess the effect of pore fluid on the fabric formed by soils as they settle in a liquid environment [83]. Figure 6a shows the volume change as a function of time for a 50%/50% diatomaceous earth/montmorillonite mixture in a 0.01 M NaCl solution. In these tests, as the particles settle, they flocculate or aggregate forming different fabrics. The volume of the sedimented material at the bottom of the column decreases gradually as the effective stress increases and the solid skeleton consolidates. Sedimentation tests continued until the sedimentation volume no longer changed. The time to reach the final sedimented volume is longer with the higher proportion of montmorillonite and lower NaCl concentrations. This response is expected for soils with lower coefficients of consolidation [15, 56]. Also, the final height of the settled material is a function of the thickness of the diffuse double layer $\vartheta \propto \sqrt{\left[\varepsilon_r \cdot T / (c_0 \cdot z)^2 \right]}$ (where ϑ is the diffused double layer thickness, ε_r is the relative permittivity of the pore fluid, T is the absolute temperature, c_0 is the fluid concentration, and z is the ion valence), and final fabric of the sedimented soil. The higher NaCl concentration in the solution reduces the thickness of the diffuse double layer, and the final sedimentation volume also decreases. This effect is most significant in the montmorillonite and becomes less relevant as diatom content increases in the mixture (Fig. 6b). However, for NaCl concentrations of 1.0 M, the final sedimented volume was practically independent of all soil mixtures. The diffused

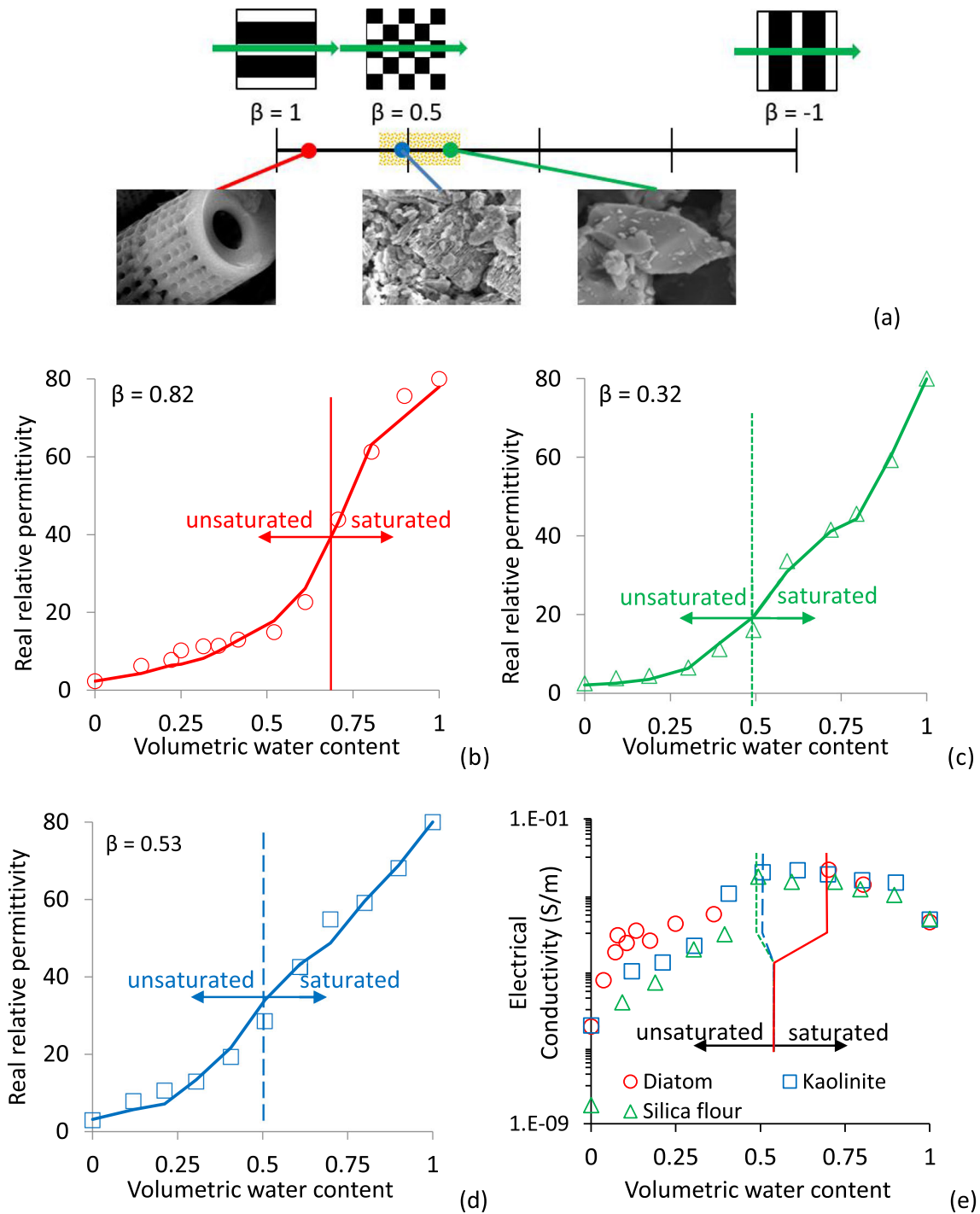


Fig. 4 a Conceptual description of particle arrangement factor β (Eq. 1). 10 MHz real relative permittivity of fine-grained soils vs. volumetric water content for **b** diatomaceous earth, **c** silica flour, and **d** kaolinite specimens. **e** Electrical conductivity of soils vs. volumetric water content

double layer became much thinner, and the mixture behaved like coarse-grained soils. Palomino et al. [81] indicated that when the NaCl concentration increases, the final fabric of the mixture transitions from being controlled by the chemistry to a simple geometric effect. During this transition, the impact of electrical charges on the edges and

faces reduces (especially for the thin montmorillonite particles). Then, the diffused double layer shrinks, and the volume decreases as the particles flocculate in the form of edge-to-edge or face-to-face [25, 56, 81, 94].

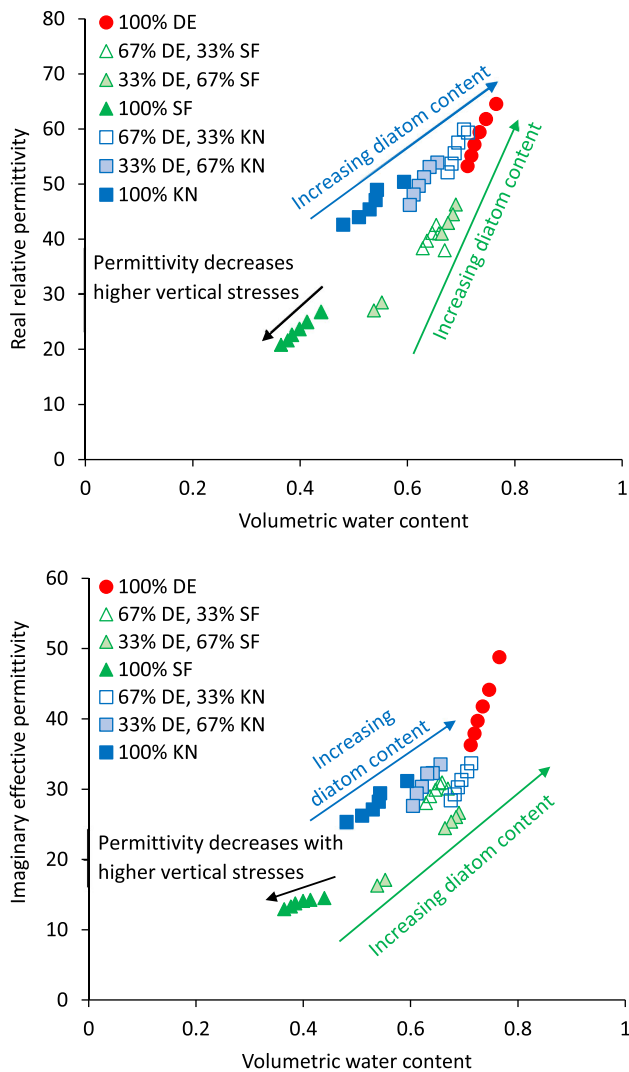


Fig. 5 Evolution of the effective real and imaginary relative permittivities of saturated fine-grained soil mixes with diatoms as the effective vertical stress increases during compression tests

4.3 Atterberg limits of fine-grained soil under varying pore fluid salt concentration

Figure 7 presents the Atterberg Limits of the silica flour, kaolinite, and montmorillonite mixtures as a function of the diatom content and the NaCl concentration in the pore fluid. Again, there are clear trends in the results. The Atterberg limits of diatomaceous earth specimens are insensitive to changes in the NaCl concentration. Despite the diatoms' high specific surface area, their low surface charge density results in thin diffused double layers that do not change with dissolved salts [32]. Still, diatomaceous earth shows higher Liquid Limits than kaolinite and silica flour as diatom's internal porosity stores most of the water.

Montmorillonite clays have large net negative charge density (about 20 to 50 times larger than kaolinite—[17])

and large specific surface area (400 to 800 m²/g—[94]), and relatively weak van der Waal forces binding the particle layers. As a result, montmorillonite attracts large amounts of water and yields high Liquid Limits (about 300 with deionized water). In addition, the diffuse double layer of montmorillonite dramatically decreases with increasing NaCl concentration. Consequently, the Liquid Limit decreases from over 300 for deionized water to 95 for 1 M NaCl solution (Fig. 7 and Table 4). However, the Plastic Limits do not depend on the pore fluid NaCl concentration. Of the materials tested here, montmorillonite specimens show the most significant volume change when the water content decreases from the Liquid Limit to the Shrinkage Limit (volume change ranges from 84% for deionized pore fluid to 56% for 1 M NaCl pore fluid—Figs. 7 and 8).

While the Liquid Limit is highest for the montmorillonite specimen, the Shrinkage Limit is highest for diatomaceous earth, as documented in Fig. 7. This response results from montmorillonite adsorbing large quantities of water on the particles' outer surfaces and interlayer spaces. Then, as the water content decreases, the montmorillonite shrinks. On the other hand, as diatoms absorb large quantities of water in their internal porosity when the water leaves the intra-porous, the diatomaceous earth does not change its volume. Therefore, the Shrinkage Limit in diatomaceous earth is larger than those for montmorillonite and kaolinite, as increasing amounts of water are needed for diatomaceous earth to change its volume. Furthermore, since water removal in diatomaceous earth does not result in significant volume changes, shrinking and cracking are minimal when transitioning from the Liquid Limit to the Shrinkage Limit (Fig. 8).

Furthermore, as mixtures increase their diatom content, their Shrinkage Limits increase. The influence of diatomaceous earth is most significant in the mixes with montmorillonite (Fig. 7). In addition, we observed that shrinkage cracks in the montmorillonite mixture for all tested pore fluids became thinner or disappeared when mixed with diatoms.

The reduction of shrinkage with the presence of diatoms has important engineering implications. For example, while montmorillonite clays have low hydraulic conductivity, they tend to shrink when drying or when subjected to salt-soluble pore fluids. This shrinking creates cracks and pathways through which leachate can more easily seep. Then, the addition of diatomaceous earth could improve the performance of landfill caps and liners. That is, shrinkage cracks in clay liners triggered by the reduction in moisture or the increase in chemical concentration may be controlled by adding diatoms. Furthermore, while diatoms may increase the hydraulic conductivity of the clay mixture, they also create a more stable structure, reducing

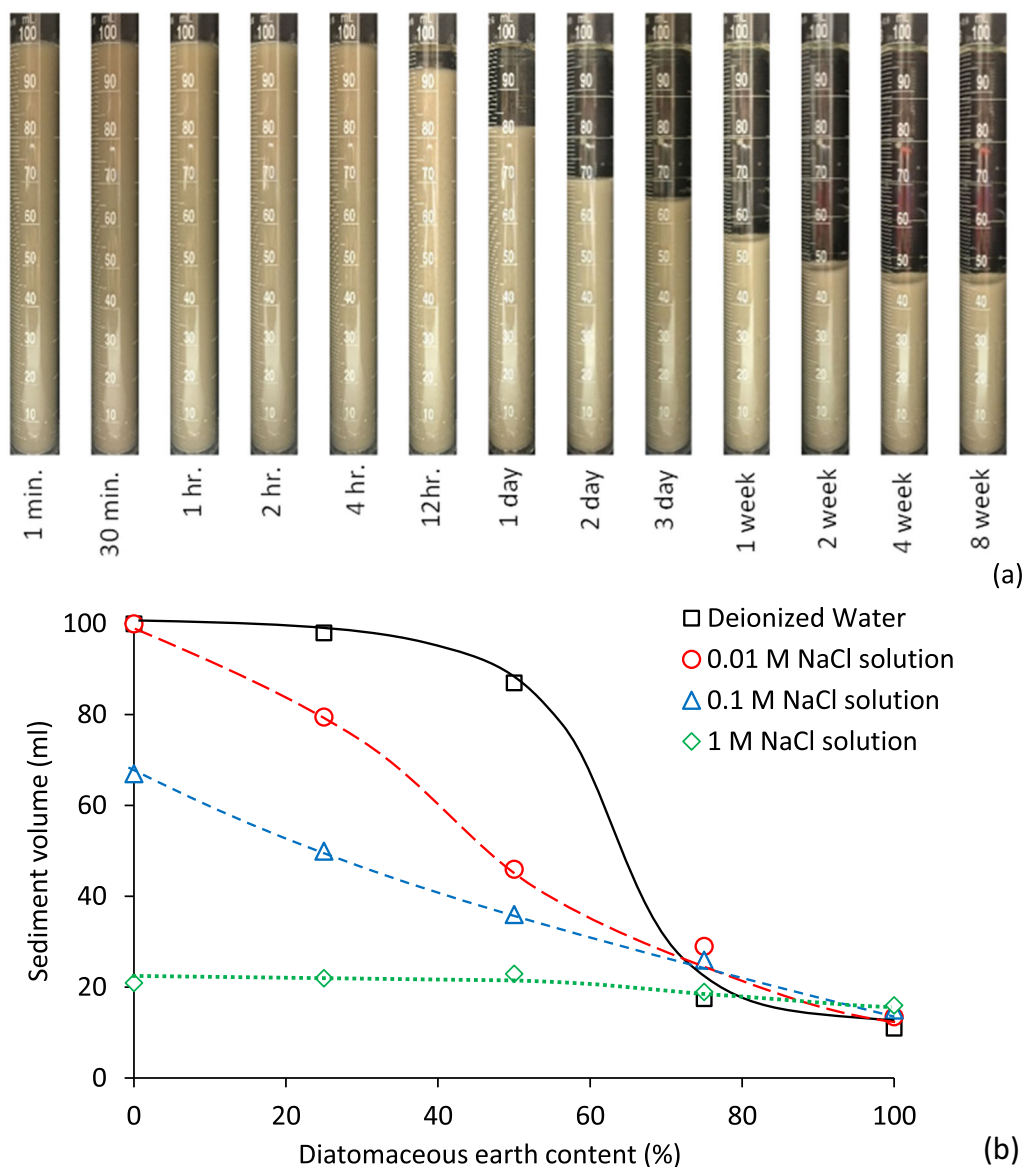


Fig. 6 **a** Sedimentation evolution for 50% diatoms and 50% montmorillonite mixture in 0.01 M NaCl pore fluid. **b** Final sediment volume for diatomaceous earth and montmorillonite mixtures in different NaCl concentration pore fluid solutions

volume change and improving the reliability of cap and liner systems.

The changes in pore fluids and the mixtures' diatom content shift the position of the soils on the Casagrande's Plasticity chart. Kaolinite and silica flour increase their Liquid Limit with the addition of diatoms (Fig. 9a). However, increasing NaCl pore fluid concentration does not affect the classification of kaolinite (clay-like behavior) and silica flour (silt-like behavior) mixtures. However, increasing the NaCl concentration in the pore fluid causes a transition in the montmorillonite response towards a kaolinite-type behavior. As a result, increasing the NaCl concentration in the pore fluid in the montmorillonite shifts its behavior by reducing the plasticity of the mixtures

(Fig. 9b). Finally, Fig. 9c documents how the Atterberg Limits of silica flour, kaolinite, and montmorillonite change as a function of diatomaceous earth content when deionized water is the pore fluid. Silica flour mixtures (with similar mineralogy to those of the fossilized diatoms) increase in Liquid Limit and Plasticity Index as the water is absorbed internally by the diatom particles. However, as the diatomaceous earth content increases, kaolinite and montmorillonite show more complex behavior. The mixtures of kaolinite and montmorillonite cross the line "A" in Casagrande's Plasticity chart when the diatom content is 33% and 70%, respectively. The mixture transitions from clay-like behavior to a more silt-like response at those points. As kaolinite is less plastic than montmorillonite, the

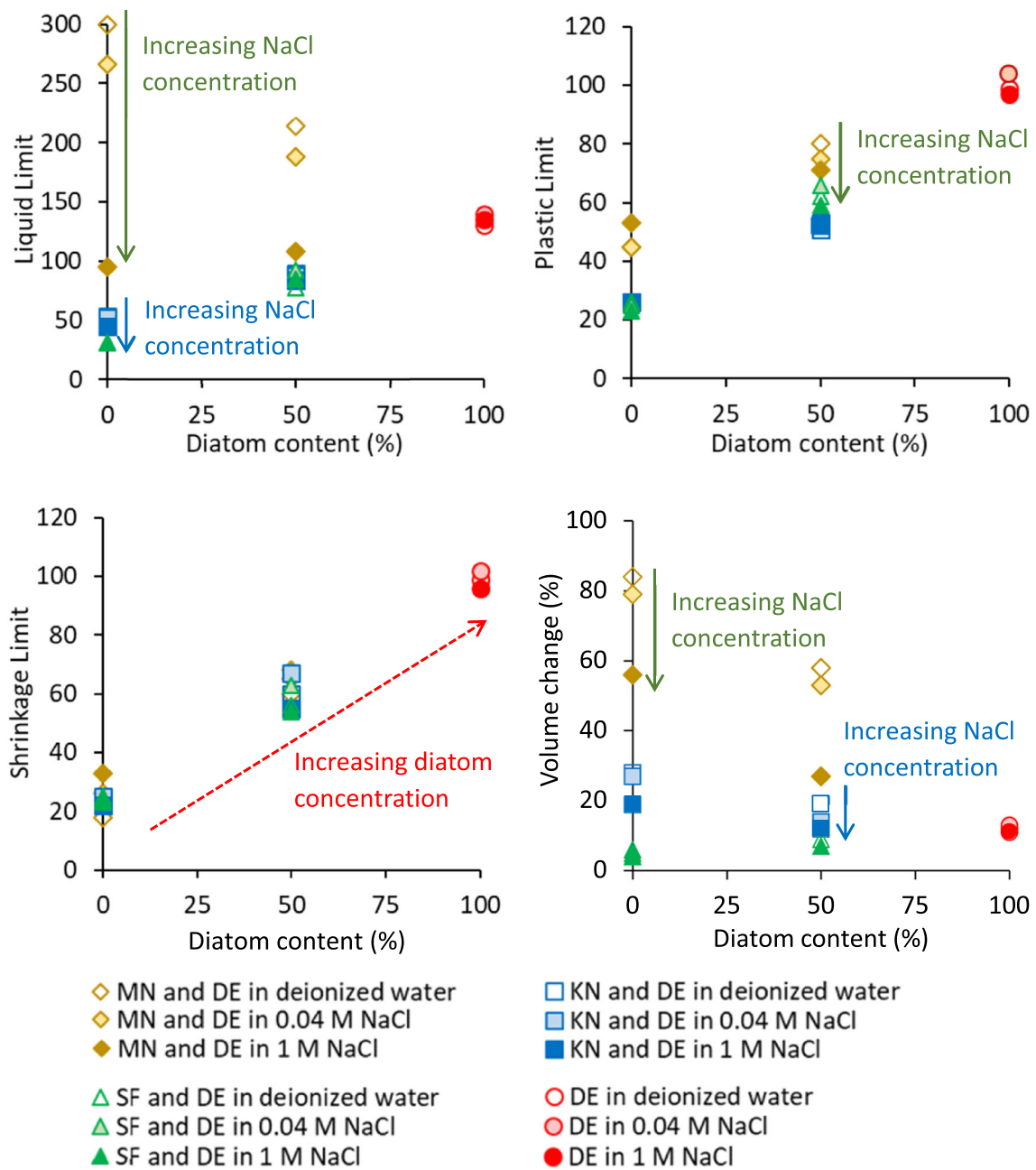


Fig. 7 Atterberg limits of soil mixtures as a function of diatom content and NaCl concentrations. The volume change of the mixture tends to transition from the Liquid Limit to the Shrinkage Limit

relative quantity of diatoms needed for this transition are smaller. Then, the transition becomes even more pronounced as the diatomaceous earth content increases.

4.4 Physical properties of abraded and crushed fine-grained soils

4.4.1 Abrasion

We measured the Atterberg Limits of soil mixtures after completing the Los Angeles abrasion and oedometer tests. We evaluated the effect of intra and interparticle porosity changes on index properties after particle degradation and crushing. The fine-grained soil particles were abraded in

Table 4 Atterberg Limits results for three fine-grained soils and mixtures with different NaCl pore fluid concentrations

	Liquid limit	Plasticity index	Void ratio	Shrinkage limit	Volume change (%)
<i>Pore fluid: deionized water</i>					
Diatomaceous earth	130	30	0.68	99	12
Silica flour	30	5	0.4	25	6
Kaolinite	53	27	0.41	22	28
Montmorillonite	300	255	0.29	18	84
50% Di + 50% Si	77	15	0.60	56	9
50% Di + 50% Mo	214	134	0.60	60	58
50% Di + 50% Ka	90	39	0.59	48	19
<i>Pore fluid: 0.04 M NaCl</i>					
Diatomaceous earth	140	36	0.7	102	13
Silica flour	31	6	0.41	24	5
Kaolinite	52	26	0.4	25	27
Montmorillonite	266	221	0.28	26	79
50% Di + 50% Si	92	26	0.61	57	7
50% Di + 50% Mo	188	113	0.60	65	53
50% Di + 50% Ka	88	36	0.60	50	14
<i>Pore fluid: 1 M NaCl</i>					
Diatomaceous earth	135	38	0.68	96	11
Silica flour	31	8	0.41	23	4
Kaolinite	45	19	0.42	25	19
Montmorillonite	95	42	0.34	33	56
50% Di + 50% Si	85	26	0.62	58	7
50% Di + 50% Mo	108	37	0.60	68	27
50% Di + 50% Ka	84	31	0.60	55	12

the Los Angeles Test machine during increasing times (from 1 to 24 h.) Table 5 and Fig. 10 summarize these results. We measured the shift in grain size distribution using the hydrometer test.

The pre and after-Los Angeles Tests' mean particle size d_{50} showed a decrease from 8.3 to 2.7 μm for diatomaceous earth, from 13.3 to 5.0 μm for silica flour, and from 0.8 to 0.3 μm for montmorillonite. However, the mean particle size of kaolinite appeared to increase from 2.4 to 35.6 μm . During the abrasion process, diatomaceous earth's physical and mechanical properties are the most affected among the soils tested: Liquid and Plastic Limits decreased from 130 to 57 and 99 to 40, respectively (Table 6). These changes are due to the reduction of internal porosities angularity of the particles (Fig. 10a—[42]). As a result, the diatomaceous earth, classified initially as MH in the Casagrande's Plasticity Chart, shifts to ML as particles undergo the abrasion process (Fig. 11).

Furthermore, the silica flour shifts its response from ML toward the transitional CL-ML type when the soil is placed under more extended Los Angeles Test periods (Fig. 10b, Fig. 11). During the abrasion process, the Atterberg Limits of silica flour decrease due to a decrease in the angularity

in the particles [58, 98] even when the mean particle size became smaller (Table 5—[42, 104]). However, those changes are minor and do not change from ML classification (Fig. 11). The Atterberg Limits of montmorillonite also decreased after 24 h. of abrasion time (Table 6). However, these changes cannot be explained just by the grain size changes or the particles' angularity. During the Los Angeles Test, we hypothesize that the abrasion process increases the time needed for the montmorillonite particles to hydrate fully. If the particles are not completely hydrated, the Liquid Limits will appear to decrease relative to the unabraded particles. Alternately, the masses of Fe and Al increased in the montmorillonite (as determined by X-ray refraction tests—Tables 6 and 7). So, we further hypothesize that adding free cations to the particles' surfaces contributes to the decrease in the measured Atterberg Limits. Our results indicate that montmorillonite gradually transitions from CH to MH as the Los Angeles Test time increases.

In contrast, abrasion appears to increase the mean particle size of kaolinite from 2.4 μm to 35.6 μm when measured using the hydrometer analysis (Table 5, Fig. 10c). The SEM images show that while kaolinite

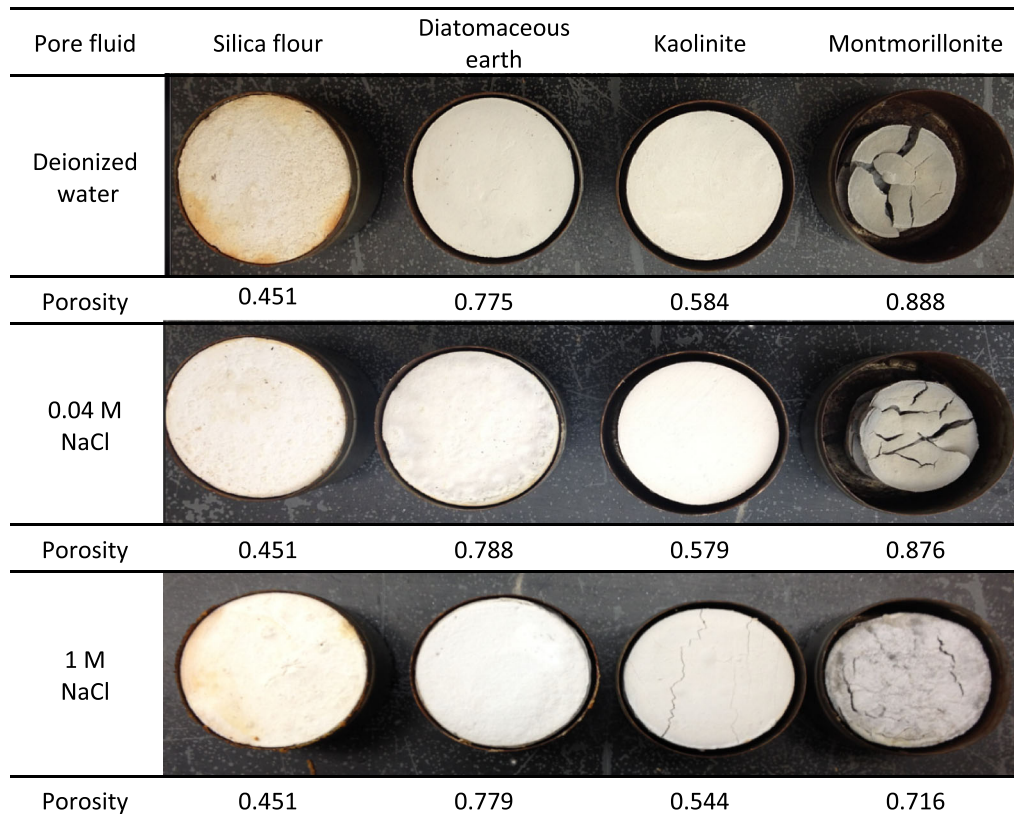


Fig. 8 Formation of cracks during volume change in different fine-grained soils

booklets break during the abrasion, individual particles press and bond together by the abrasion process, forming larger face-to-face aggregates. The dispersant used in the hydrometer test appears ineffective in completely separating these aggregates, resulting in larger particle sizes. Accordingly, the Liquid Limit decreases with increasing abrasion time, and the classification shifts from CH to ML (from just above the “A” line to just below the “A” line) after 24 h of abrasion (Fig. 11).

4.4.2 Compression

Figure 12 shows the SEM images of diatomaceous earth during increasing oedometer vertical effective stresses. Particle crushing was observed as the effective vertical stress increased, gradually shifting diatoms’ physical and mechanical properties to behave more like silica flour (Fig. 11). Figure 13a presents the log of effective stress vs. void ratio results for diatomaceous earth, silica flour, kaolinite, and selected mixtures during confined compression tests. The tested materials have different compression indices and initial void ratios; each mix represents a different soil type. The measured compression index increases with a higher initial void ratio and greater diatomaceous earth content. The compression index remains relatively

constant during loading until about 2 MPa vertical stress. Then, there is a sudden increase in the compression index (Fig. 13a). However, there is no change in the compression index in silica flour and kaolinite specimens with no diatom content. The difference in this mechanical response is due to the crushing of diatom particles (that occurs between 2 and 4 MPa—Fig. 13a). Beyond 4 MPa, the compression index appears to stabilize again, as most fossilized diatoms have already been crushed. This behavior was also confirmed by observing that the increase in the compression index is greater with increasing diatom content (Fig. 13b).

4.5 Evaluation of porosity changes

Mercury intrusion tests assess the change in the pore size distribution of the diatomaceous earth with increasing compression stresses. As the effective vertical stress increases from 0 to 2 MPa, the interparticle porosity decreases as the distance between particles decreases and a few diatoms crush (Fig. 14). As a result, the pore fraction percentage at pore diameters 0.013, 0.18, and 0.35 μm increased linearly up to 2 MPa, and the 0.77- μm pore diameter decreased without changing the fraction percentage. When particles rearrange, pore fractions change even with minor particle crushing [47]. However, subtle

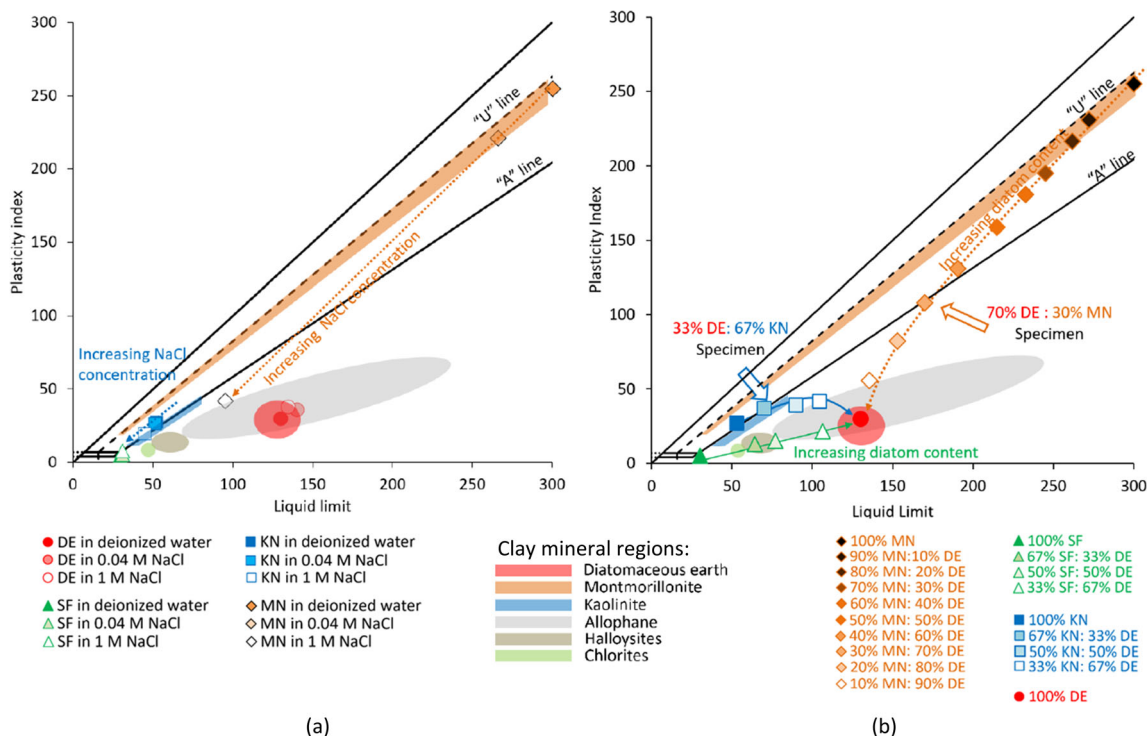


Fig. 9 The response of soil mixtures under different chemical environments and increasing diatoms content. **a** As the NaCl concentration in the solution increases, kaolinite and montmorillonite become less plastic, while diatom and silica flour do not change their plasticity. **b** Adding diatom increases the Liquid Limit in kaolinite and silica flour mixes; however, it reduces the Liquid Limit in montmorillonite. The pore fluid in these tests is deionized water

Table 5 Mean particle size d_{50} of each fine-grained subjected to the Los Angeles abrasion and oedometer test

d_{50} (μm)	Natural	Los Angles test			
		1 h	4 h	12 h	24 h
Diatomaceous earth	8.3	7.4	6.2	3.4	2.7
Silica flour	13.3	12.4	9.7	5.8	5.0
Kaolinite	2.4	2.4	4.4	33.3	35.6
Montmorillonite	0.8	1.5	0.8	0.4	0.3
d_{50} (μm)	Natural	Confined compression test			
		1 MPa	2 MPa	4 MPa	8 MPa
Diatomaceous earth	8.3	7.1	6.6	5.4	4.7
Silica flour	13.3	13.0	13.1	13.0	12.8
Kaolinite	2.4	2.5	2.4	2.5	2.6

but essential changes occur when the effective vertical stress increases beyond 2 to 4 MPa, and particle crushing occurs. As the particles crush between 2 and 4 MPa, the pore diameters fraction percentage of 0.013, 0.18, and 0.35 μm significantly increase. The decrease in mean particle size d_{50} also indicates that particle crushing occurs as the

stress in the diatomaceous earth increases from 2 to 8 MPa (Table 5).

4.5.1 Particle breakage discussion

When diatomaceous earth particles break under compressive stresses, they lose their ability to store water within the

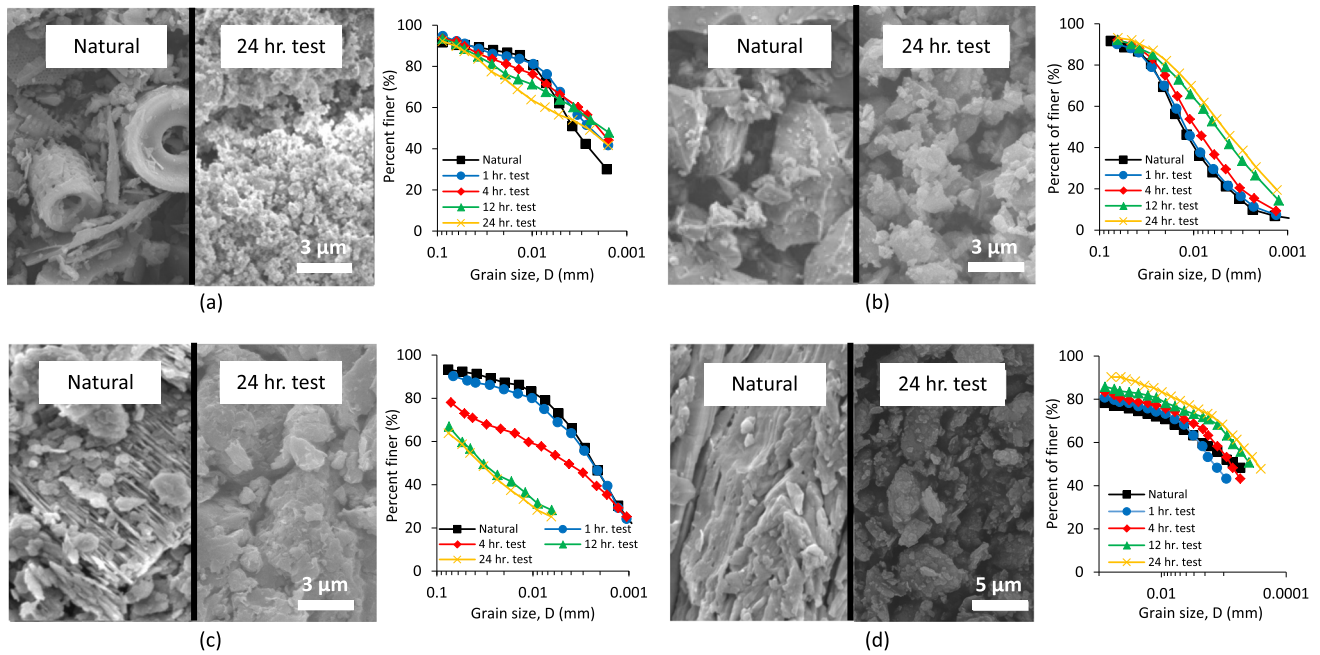


Fig. 10 Effect of abrasion on the fine-grained soil particles. High-resolution SEM images comparing natural and abraded specimens after 24 h of Los Angeles test for **a** diatomaceous earth, **b** silica flour, **c** kaolinite, and **d** montmorillonite

Table 6 Atterberg Limits after Los Angeles abrasion and oedometer tests

	Diatomaceous earth		Silica flour		Kaolinite		Montmorillonite	
	LL	PI	LL	PI	LL	PI	LL	PI
Natural	130	30	30	5	53	27	300	255
<i>Los Angeles test</i>								
1 h	118	28	29	5	51	26		
4 h	103	36	27	5	45	19		
8 h	76	25	26	6				
12 h	67	22	25	6	40	12		
24 h	57	17	24	6	38	12	163	105
<i>Oedometer test</i>								
1 MPa	114	31	31	5	53	26		
2 MPa	108	27	30	5	54	25		
4 MPa	92	24	31	5	53	27		
8 MPa	83	16	32	5	54	27		

particles, and the Atterberg Limits decrease (Table 7). In contrast, the Liquid Limits of kaolinite and silica flour specimens are unaffected by increased compression stresses. Furthermore, particles smaller than 0.074 mm are not typically susceptible to breakage during compression [61]. Silica flour particles require about 30 MPa for particle crushing [59]. However, due to their unique hollow structure, the diatoms are susceptible to breakage even when particles are smaller than 0.074 mm and below 30 MPa. Hamm et al. [44] found that diatoms can support a force of

about 750 μN before they break. For a 3-MPa isotropic effective stress, we calculated forces of 276 μN would cause crushing in a simple cubic packing of particles of diameter $d = 8.3 \mu\text{m}$, void ratio $e = 2.4$, and coordination number $c_n = 8$ [94]. Besides, in the case of soils containing diatoms, physical properties may change during compression, requiring attention to the effect of high stresses on the engineering properties of diatomaceous earth or soils containing diatoms in geotechnical engineering projects.

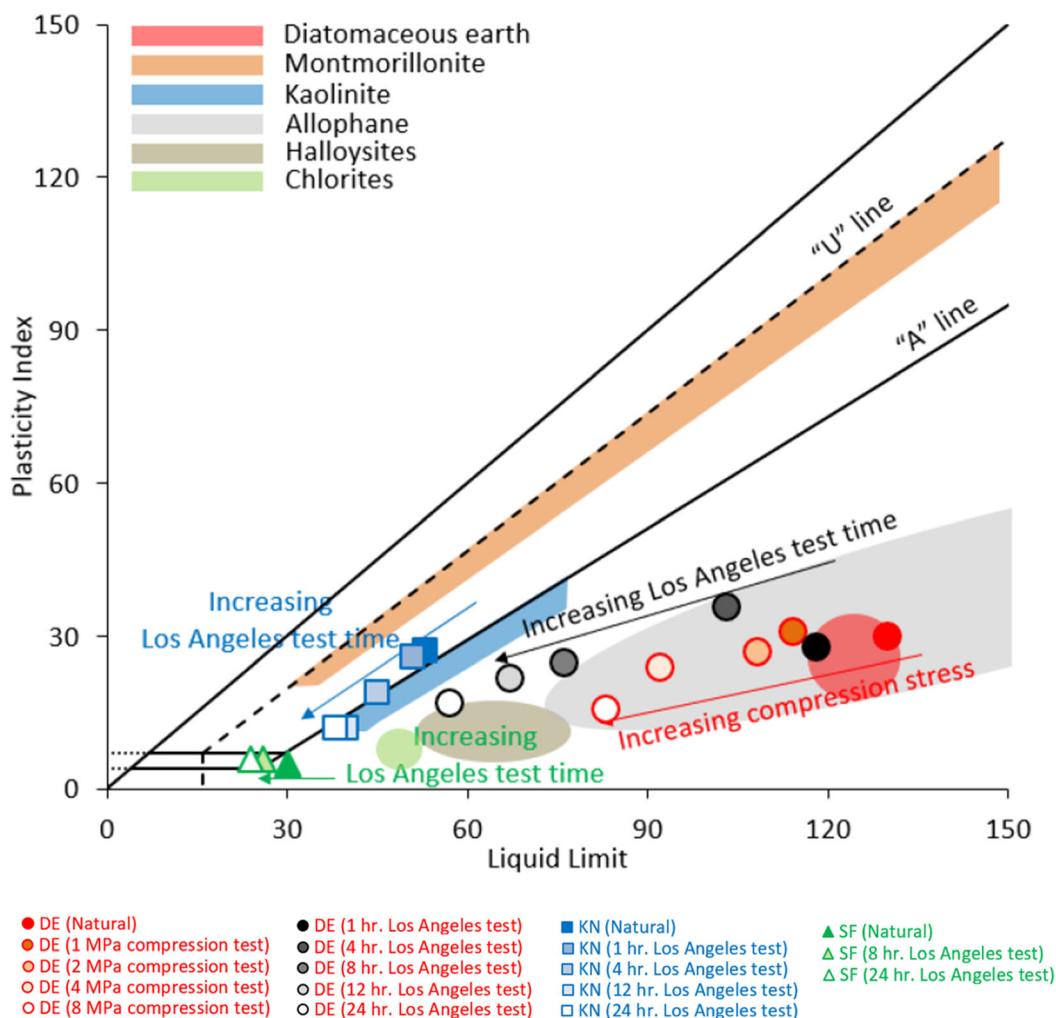


Fig. 11 Shifts in the Casagrande Chart as abrasion time during Los Angeles Tests and particle crushing in the oedometer test

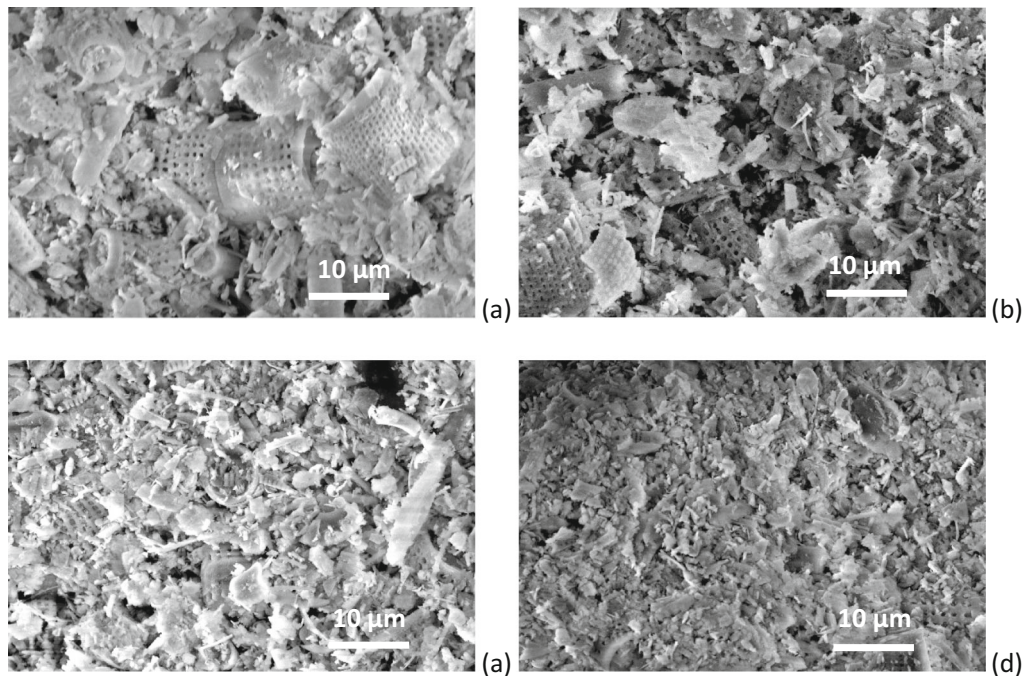
5 Conclusions

Fossilized diatoms in artificial fine-grained soil mixtures influence the overall behavior of soils. This study attempted to answer the question: What percentage of diatomaceous earth in a fine-grained soil mixture will control the overall properties? Our results show that simple physical and index tests capture the effect of fossilized diatoms in soils:

- While diatomaceous earth and silica flour particles have similar mineral compositions, the estimated 10-MHz relative dielectric permittivity at zero porosity of fossilized diatoms is similar to the dielectric permittivity of kaolinite. This is because the water entrapped in the hollow structure of diatoms increases the measured permittivity above the permittivity of the silica flour. Furthermore, higher fossilized diatom contents in saturated mixtures yield higher permittivities for similar void ratios than other fine-grained soils.
- Sedimentation volumes of fine-grained soils decrease with higher diatoms content and NaCl concentration in the pore fluid. The sedimented volumes are controlled mainly by the thickness of the diffuse double layer in the different mixtures. Fossilized diatoms form a thin diffuse double-layer thickness that is insensitive to changes in the salt concentration of the pore fluid. In contrast, the thickness of the diffused double layer of clay mineral particles reduces with salt concentrations in the pore fluid.
- Atterberg Limits results show that mixtures with high diatom content retain high quantities of water even under high NaCl-concentration pore fluids: diatoms store most pore fluid in their hollow structure. So, their response is independent of the chemical concentration in the pore fluid. Furthermore, diatomaceous earth does not shrink when drying, improving the mixture stability when mixed with other fine-grained soils. So, adding diatoms might benefit landfill liners and caps where

Table 7 Soils' chemical composition during increasing Los Angeles Abrasion testing times

Element	Weight composition (%)			
	Natural	1 h	4 h	24 h
<i>(a) Diatomaceous earth</i>				
O	60.19	61.59	61.92	62.19
Si	37.13	35.09	34.93	33.73
Al	1.87	1.88	1.87	2.14
Fe	0.54	0.77	0.8	0.98
Ca	0.27	0.36	0.23	0.49
Mg		0.32	0.26	0.31
K				0.15
<i>(b) Montmorillonite</i>				
O	56.38	56.84	57.12	58.61
Si	27.18	26.56	26.14	24.68
Al	8.18	8.20	8.26	8.28
Fe	3.26	3.42	3.48	3.52
Na	1.57	1.5	1.52	1.48
Mg	1.27	1.28	1.30	1.33
Ca	1.18	1.22	1.22	1.25
S	0.47	0.45	0.42	0.43
K	0.35	0.37	0.37	0.36
Ti	0.17	0.16	0.16	0.16

**Fig. 12** Effect of oedometer stress on the fossilized diatom particles as documented by SEM images: **a** 1 MPa, **b** 2 MPa, **c** 4 MPa, and **d** 8 MPa vertical effective stress

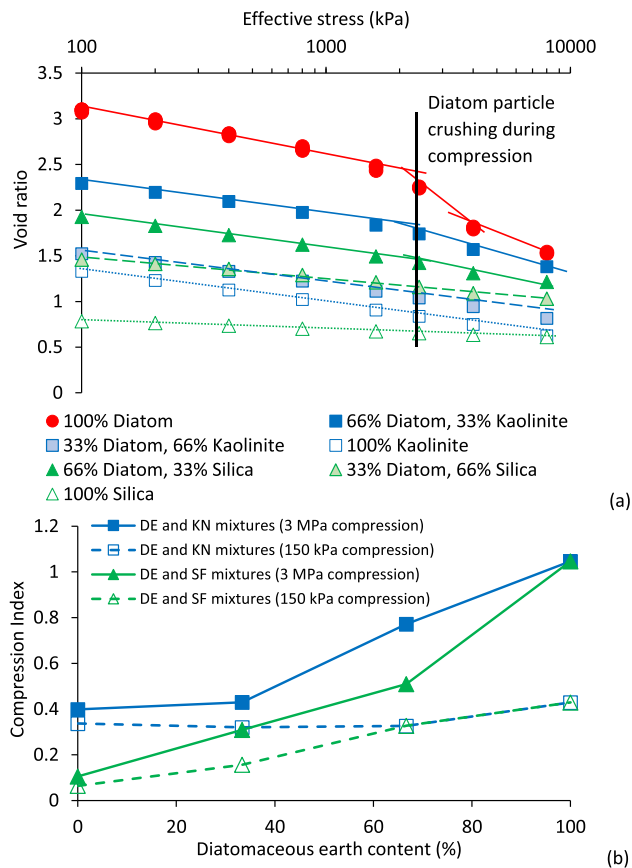


Fig. 13 **a** Effect of oedometer stress on the compression index for different combinations of fine particles percentage. **b** Compression index at 150 kPa and 3 MPa vertical effective stress for soil specimens with diatom content

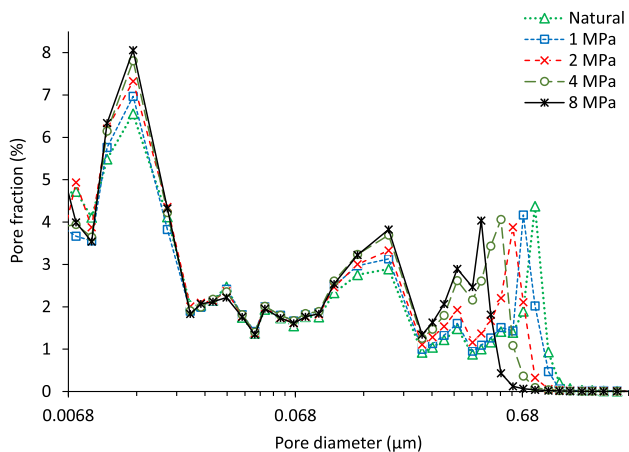


Fig. 14 Mercury-intrusion determined pore fractions as a function of the pore diameter from diatomaceous earth specimens collected during confined compression tests

chemical leachates and drying conditions tend to crack and deteriorate their performance.

- The internal porosity of diatoms is easily affected by abrasion and particle crushing, decreasing the water

storage ability of fossilized diatoms. Then, when fossilized diatoms are abraded and crushed, Liquid and Plastic Limits fall, and the compression index increases.

All our results indicate the feasibility of simple physical, electromagnetic, and mechanical tests to characterize the presence of fossilized diatoms and assess their unique effect on the behavior of both natural and artificial soils. Furthermore, these tests provide insight into the pros (i.e., high friction angle and volumetric stability under water content changes and high-concentration electrolyte environments) and cons (i.e., potential collapse under relatively low compression stresses and low abrasion resistance) of using soils with diatom content in geotechnical and geoenvironmental engineering projects.

Acknowledgements The Wisconsin Highway Research Program partially supported Dr. Jeongki Lee's studies. The authors also acknowledge the support provided by the Civil and Environmental Engineering departments at the University of Wisconsin-Madison and the University of Tennessee-Knoxville.

Data availability The datasets generated and analyzed during this current study are available from the corresponding author on reasonable request.

References

1. Akin I, Likos W (2014) Specific surface area of clay using water vapor and EGME sorption methods. *Geotech Test J* 37(6):1016–1027
2. ASTM (2017) C131: Standard test method for resistance to degradation of small-size coarse aggregate by Abrasion and Impact in the Los Angeles Machine. ASTM International, West Conshohocken, PA
3. ASTM (2018) C2435: Standard Test Method for Determination of Pore Volume and Pore Volume Distribution of Soil and Rock by Mercury Intrusion Porosimetry. ASTM International, West Conshohocken, PA
4. ASTM (2018) D4318: Standard test methods for liquid limit, plastic limit, and plasticity index of soils. ASTM International, West Conshohocken, PA
5. ASTM (2018) D4404: Standard test method for determination of pore volume and pore volume distribution of soil and rock by mercury intrusion porosimetry. ASTM International, West Conshohocken, PA
6. ASTM (2018) D4943: Standard test method for shrinkage factors of cohesive soils by the water submersion method. ASTM International, West Conshohocken, PA
7. ASTM (2019) D150: Standard test methods for AC loss characteristics and permittivity (dielectric constant) of solid electrical insulation. ASTM International, West Conshohocken, PA
8. ASTM (2020) C2435: standard test methods for one-dimensional consolidation properties of soils using incremental loading. ASTM International, West Conshohocken, PA
9. ASTM (2021) D7928: standard test method for particle-size distribution (gradation) of fine-grained soils using the sedimentation (hydrometer) analysis. ASTM International, West Conshohocken, PA

10. ASTM (2023) D5550: standard test method for specific gravity of soil solids by gas pycnometer. ASTM International, West Conshohocken, PA
11. Attia AM, Fratta D, Bassiouni Z (2008) Irreducible water saturation from capillary pressure and electrical resistivity measurements. *Oil Gas Sci Technol-Rev de l'IFP* 63(2):203–217
12. Aydin AC, Gul R (2007) Influence of volcanic originated natural materials as additives on the setting time and some mechanical properties of concrete. *Constr Build Mater* 21(6):1277–1281
13. Azo Materials (2020) Company website: Silica - Silicon Dioxide (SiO₂) <https://www.azom.com/properties.aspx?ArticleID=1114> Accessed 27 May 2020
14. Been K, Sills GC (1981) Self-weight consolidation of soft soils - an experimental and theoretical study. *Geotechnique* 31(4):519–535
15. Brady NC (1984) The nature properties of soils. 9th Edition, Collier Macmillan Canada, Inc
16. Bryant WR, Rack FR (1990) 17. Consolidation characteristic of Weddell sea sediments: results of ODP LEP 113. *Proc ODP Sci Results* 113:211–223
17. Burger CA, Shackelford CD (2001) Evaluating dual porosity of pelletized diatomaceous earth using bimodal soil–water characteristic curve functions. *Can Geotech J* 38(1):53–66
18. Caicedo B, Mendoza C, Lizcano A, Lopez-Caballero F (2019) Some contributions to mechanical behaviors of lacustrine deposit in Bogotá, Colombia. *J Rock Mech Geotech Eng* 11(4):837–849
19. Caicedo B, Zuluaga D, Slebi C (2019) Effects of micro-features of fossil diatom on the macroscopic behaviour of soils. *Géotech Lett* 9(4):322–327
20. Cartnick K, Merwin R (2004) Franklin lakes: creating a permanent solution for a limited seasonal need. *J Am Water Works Assoc* 96(9):34–37
21. Cascante G, Santamarina JC (1996) Interparticle contact behavior and wave propagation. *J Geotech Eng* 122(10):831–839
22. Cerato AB, Lutenege AJ (2002) Determination of surface area of fine-grained soils by the ethylene glycol monoethyl ether (EGME) method. *Geotech Test J* 25(3):315–321
23. Chen J, Anandarajah A, Inyang H (2000) Pore fluid properties and compressibility of kaolinite. *J Geotech Geoenviron Eng* 126(9):798–807
24. Chester R, Elderfield H (1968) The infrared determination of opal in siliceous deep-sea sediments. *Geochim Cosmochim Acta* 32(10):1128–1140
25. Cloyd RA, Dickinson A (2005) Effects of growing media containing diatomaceous earth on the fungus gnat *Bradysia* sp. nr. *coprophila* (Lintner) (Diptera: Sciaridae). *HortScience* 40(6):1806–1809
26. Day RW (1995) Engineering properties of diatomaceous fill. *J Geotech Eng* 121(12):908–910
27. DeMaster DJ (1981) The supply and accumulation of silica in the marine environment. *Geochem Cosmochim Acta* 45(10):1715–1732
28. Diaz-Rodríguez JA, Gonzalez-Rodríguez R (2013) Influence of diatom microfossils on soil compressibility. In: 18th International conference on soil mechanics and geotechnical engineering, 325–328
29. Diaz-Rodríguez JA, Leroueil S, Aleman JD (1992) Yielding of Mexico City clay and other natural clays. *J Geotech Eng* 118(7):981–995
30. Dixit S, Van Cappellen P (2002) Surface chemistry and reactivity of biogenic silica. *Geochim Cosmochim Acta* 66(14):2559–2568
31. Eggimann DW, Betzer PR (1976) Decomposition and analysis of refractory oceanic suspended materials. *Anal Chem* 48(6):886–890
32. Eggimann DW, Manheim TF, Betzer RP (1980) Dissolution and analysis of amorphous silica in marine sediments. *J Sediment Petrol* 50(1):215–225
33. Einsele G (1990) Deep-reaching liquefaction potential of marine slope sediments as a prerequisite for gravity mass flows? (results from the DSDP). *Mar Geol* 91(4):267–279
34. Eisma D, Van der Gaast SJ (1971) Determination of opal in marine sediments by X-ray diffraction. *Neth J Sea Res* 5(3):382–389
35. Escalera E, Garcia G, Teran R, Tegman R, Antti ML, Oden M (2015) The production of porous brick material from diatomaceous earth and Brazil nut shell ash. *Constr Build Mater* 98:257–264
36. Fam M (1995) Study of physico-chemical processes in geomaterials with mechanical and electromagnetic waves. Ph.D. Thesis. University of Waterloo. Waterloo, Canada
37. Fragoulis D, Stamatakis MG, Papageorgiou D, Chaniotakis E (2005) The physical and mechanical properties of composite cements manufactured with calcareous and clayey Greek diatomite mixtures. *Cement Concr Compos* 27(2):205–209
38. Fulton GP (2000) Diatomaceous earth filtration for safe drinking water. American Society of Civil Engineers, Reston
39. Greenspan HP, Ungarish M (1982) On hindered settling of particles of different sizes. *Int J Multiph Flow* 8(6):587–604
40. Guo P, Su X (2007) Shear strength, interparticle locking, and dilatancy of granular materials. *Can Geotech J* 44(5):579–591
41. Haigh SK, Vardanega PJ, Bolton MD (2013) The plastic limit of clays. *Geotechnique* 63(6):435–440
42. Hamm CE, Merkel R, Springer O, Jurkojc P, Maier C, Prechtel K, Smetacek V (2003) Architecture and material properties of diatom shells provide effective mechanical protection. *Nature* 421:841–843
43. Hardin BO (1985) Crushing of soil particles. *J Geotech Eng* 111(10):1177–1192
44. Hoang NQ, Kim SY, Lee JS (2022) Compressibility, stiffness and electrical resistivity characteristics of sand–diatom mixtures. *Géotechnique* 72(12):1068–1081
45. Hong J, Tateishi Y, Han J (2006) Experimental study of macro- and micro behavior of natural diatomite. *J Geotech Geoenviron Eng* 132(5):603–610
46. Israelachvili JN (2011) Intermolecular and surface forces. Academic Press
47. Jeffryes C, Campbell J, Li H, Jiao J, Rorrer G (2011) The potential of diatom nanobiotechnology for applications in solar cells, batteries, and electroluminescent devices. *Energy Environ Sci* 4(10):3930–3941
48. Jones SB, Wraith JM, Or D (2002) Time domain reflectometry measurement principles and applications. *Hydrol Process* 16:141–153
49. Kastic D, Kakali G, Tsivilis S, Stamatakis MG (2006) Properties and hydration of blended cements with calcareous diatomite. *Cem Concr Res* 36(10):1821–1826
50. Kietzman JH, Rodier CE (1984) Effect of diatomite filler on performance of asphalt pavements. *Transp Res Rec* 968:8–19
51. Klein KA, Santamarina JC (2003) Electrical conductivity in soils: underlying phenomena. *J Environ Eng Geophys* 8(4)
52. Klein KA, Santamarina JC (2005) Soft sediments: wave-based characterization. *J Geotech Geoenviron Eng* 5(2):147–157
53. Klein SH (1972) US Patent No. 3,705,651. Washington, DC: US Patent and Trademark Office
54. Krumbein WC (1941) The effects of abrasion on the size, shape, and roundness of rock fragments. *J Geol* 49(5):482–520

55. Lade PV, Yamamuro JA, Bopp PA (1996) Significance of particle crushing in granular materials. *J Geotech Eng* 122(4):309–316
56. Lee J (2014) Evaluation of diatomaceous earth content in natural soils for potential engineering applications. MS Thesis. University of Wisconsin-Madison. Madison, WI. USA
57. Lee KL, Farhoomand I (1967) Compressibility and crushing of granular soil in anisotropic triaxial compression. *Can Geotech J* 4(1):68–86
58. Leinen M (1976) A normative calculation technique for determining opal in deep-sea sediments. *Geochim Cosmochim Acta* 41(5):671–676
59. Leluk K, Orzechowski K, Jerie K, Baranowski A, Slonka T, Glowinski J (2010) Dielectric permittivity of kaolinite heated to high temperatures. *J Phys Chem Solids* 71(5):827–831
60. Liu X, Chen J, Li H (2006) Phase morphology and rheological properties of metallocene-catalyzed linear low-density polyethylene with a small amount of diatomite/oligomer hybrids. *J Polym Sci Part B: Polym Phys* 44(9):1287–1295
61. Losic D, Pillar RJ, Dilger T, Mitchell JG, Voelcker NH (2007) Atomic force microscopy (AFM) characterization of the porous silica nanostructure of two centric diatoms. *J Porous Mater* 14(1):61–69
62. Lundkvist M, Gangelhof U, Lunding J, Flindt MR (2007) Production and fate of extracellular polymeric substances produced by benthic diatoms and bacteria: a laboratory study. *Estuar Coast Shelf Sci* 75(3):337–346
63. Luo JJ, Daniel IM (2003) Characterization and modeling of mechanical behavior of polymer/clay nanocomposites. *Compos Sci Technol* 63(11):1607–1616
64. MacKillop AK, Moran K, Jarrett K, Farrell J, Murray D (1995) 16. Consolidation properties of Equatorial Pacific Ocean sediments and their relationship to stress history and offset in the LEG 138 composition depth sections. *Proc ODP Sci Results* 138:357–369
65. Madsen KN, Nilsson P, Sundback K (1993) The influence of benthic microalgae on the stability of a subtidal sediment. *J Exp Mar Biol Ecol* 170(2):159–177
66. Marković G, Marinović-Cincović M, Valentova H, Ilavsky M, Radovanović B, Budinski-Simendić J (2005) Curing characteristics and dynamic mechanical behavior of reinforced acrylonitrile-butadiene/chlorosulfonated polyethylene rubber blends. *Mater Sci Forum* 494:475–480
67. McAllister SD, Ponraj R, Cheng F, Edwards DB (2007) Increase of positive active material utilization in lead-acid batteries using diatomaceous earth additives. *J Power Sources* 173(2):882–886
68. McManis KL, Nataraj M (1997) Characterization of filter cake ash and applications for soil stabilization. In: *Testing soil mixed with waste or recycled materials*. ASTM International
69. Miklasz KA, Denny MW (2010) Diatom sinking speeds: Improved predictions and insight from a modified Stokes' law. *Limnol Oceanogr* 55(6):2513–2525
70. Mortlock RA, Froelich PN (1989) A simple method for the rapid determination of biogenic opal in pelagic marine sediments. *Deep Sea Res Part A. Oceanogr Res Pap* 36(9):1415–1426
71. Muller PJ, Schneider R (1993) An automated leaching method for the determination of opal in sediments and particulate matter. *Deep Sea Res Part I* 40(3):425–444
72. Odell RT, Thornburn TH, McKenzie LJ (1960) Relationships of Atterberg limits to some other properties of Illinois soils. *Soil Sci Soc Am J* 24(4):297–300
73. Or D, Wraith JM (1999) Temperature effects on soil bulk dielectric permittivity measured by time domain reflectometry: a physical model. *Water Resour Res* 35(2):371–383
74. Osmanlioglu AE (2007) Natural diatomite process for removal of radioactivity from liquid waste. *Appl Radiat Isot* 65(1):17–20
75. Ovalle C, Arenaldi-Perisic G (2021) Mechanical behaviour of undisturbed diatomaceous soil. *Mar Georesour Geotechnol* 39(5):623–630
76. Palomino AM, Burns SE, Santamarina JC (2008) Mixtures of fine-grained minerals—kaolinite and carbonate grains. *Clays Clay Miner* 56(6):599–611
77. Palomino AM, Kim S, Summitt A, Fratta D (2011) Impact of diatoms on fabric and chemical stability of diatom-kaolin mixtures. *Appl Clay Sci* 51(3):287–294
78. Palomino AM, Santamarina JC (2005) Fabric map for kaolinite: effects of pH and ionic concentration on behavior. *Clays Clay Miner* 53(3):209–222
79. Perisic GA, Ovalle C, Barrios A (2019) Compressibility and creep of a diatomaceous soil. *Eng Geol* 258:105145
80. Pokras EM (1986) Preservation of fossil diatoms in Atlantic sediment cores: control by supply rate. *Deep Sea Res Part A. Oceanogr Res Pap* 33(7):893–902
81. Portier R, Fujisaki K, Reily L, Henry C (1987a) Detoxification of contaminated groundwaters using a marine polysaccharide/diatomaceous earth packed bed biological reactor. *Oceans* 1709–1712
82. Portier R, Fujisaki K, Reily L, McMillin D (1987b) Detoxification of rinsates from aerial pesticide applications using a marine polysaccharide/diatomaceous earth packed bed biological reactor. *Oceans* 1713–1716
83. Portier RJ, Miller GP (1991) Immobilized microbe bioreactors for wastewater treatment. *Waste Manage Res* 9(5):445–451
84. Rao SM, Sridharan A, Chandrakaran S (1989) Influence of drying on the liquid limit behaviour of a marine clay. *Geotechnique* 39(4):715–719
85. Revil A (2013) Effective conductivity and permittivity of unsaturated porous materials in the frequency range 1 MHz–1 GHz. *Water Resour Res* 49(1):306–327
86. Rhoades JD, Manteghi NA, Shouse PJ, Alves WJ (1989) Estimating soil salinity from saturated soil-paste electrical conductivity. *Soil Sci Soc Am J* 53(2):428–433
87. Roth K, Schulin R, Flüeler H, Attinger W (1990) Calibration of time domain reflectometry for water content measurement using a composite dielectric approach. *Water Resour Res* 26(10):2267–2273
88. Santamarina JC, Fratta D (2003) Dynamic electrical-mechanical energy coupling in electrolyte-mineral systems. *Transp Porous Media* 50(1–2):153–178
89. Santamarina JC, Klein KA, Fam MA (2001) *Soils and waves*. Wiley, Chichester
90. Sen PN, Scala C, Cohen MH (1981) A self-similar model for sedimentary rocks with application to the dielectric constant of fused glass beads. *Geophysics* 46(5):781–795
91. Shalkevich A, Stradner A, Bhat SK, Muller F, Schurtenberger P (2007) Cluster, glass, and gel formation and viscoelastic phase separation in aqueous clay suspensions. *Langmuir* 23(7):3570–3580
92. Shiwakoti DR, Tanaka H, Tanaka M, Locat J (2002) Influences of diatom microfossils on engineering properties of soils. *Soils Found* 42(3):1–17
93. Stachowiak GW (2000) Particle angularity and its relationship to abrasive and erosive wear. *Wear* 241(2):214–219
94. Stepkowska ET, Perez-Rodriguez JL, Justo A, Soto PS, Jefferis SA (1988) Possibility of feldspar formation in bentonite suspensions during storage, drying and/or heating. *Thermochim Acta* 135:319–334
95. Stewart DI, Studds PG, Cousens TW (2003) The factors controlling the engineering properties of bentonite-enhanced sand. *Appl Clay Sci* 23(1–4):97–110

96. Tanaka M, Tanaka H (2003) Effects of diatom microfossil contents on engineering properties of soils. *International Society of Offshore and Polar Engineers* 372–377
97. Topp GC, Davis JL, Annan AP (1980) Electromagnetic determination of soil water content: measurements in coaxial transmission lines. *Water Resour Res* 16(3):574–582
98. Tsai WT, Hsien KJ, Yang JM (2004) Silica adsorbent prepared from spent diatomaceous earth and its application to removal of dye from aqueous solution. *J Colloid Interface Sci* 275(2):428–433
99. Tsomokos A, Georgiannou VN (2010) Effect of grain shape and angularity on the undrained response of fine sands. *Can Geotech J* 47(5):539–551
100. Underwood GJ, Paterson DM (1993) Seasonal changes in diatom biomass, sediment stability and biogenic stabilization in the Severn Estuary. *J Mar Biol Assoc UK* 73(4):871–887
101. Vaneesorn N, Khammanee S, Kahawong P, Danwittayakul S, Thanaboonsombut A (2009) Utilization of diatomite as a desiccant aid. In: 27th Annual Cocoa Beach conference on advanced ceramics and composites-A 268:159
102. Wagner N, Emmerich K, Bonitz F, Kupfer K (2011) Experimental investigations on the frequency-and temperature-dependent dielectric material properties of soil. *IEEE Trans Geosci Remote Sens* 49(7):2518–2530
103. Wasti Y (1987) Liquid and plastic limits as determined from the fall cone and the Casagrande methods. *Geotech Test J* 10(1):26–30
104. Wei J, Gencturk B (2018) Degradation of natural fiber in cement composites containing diatomaceous earth. *J Mater Civ Eng* 30(11):04018282
105. White WA (1949) Atterberg plastic limits of clay minerals. *Am Mineral: J Earth Planet Mater* 34(7–8):508–512
106. Wiemer G, Kopf A (2017) Influence of diatom microfossils on sediment shear strength and slope stability. *Geochem Geophys Geosyst* 18(1):333–345
107. Wroth CP, Wood DM (1978) The correlation of index properties with some basic engineering properties of soils. *Can Geotech J* 15(2):137–145
108. Xu Y, Zhang X, Liu X, Wang G (2022) Alterations of physical properties and microstructure of marine diatomite owing to variation of diatom content. *Mar Georesour Geotechnol* 41(4):376–387
109. Yilmaz B (2008) A study on the effects of diatomite blend in natural pozzolan-blended cements. *Adv Cem Res* 20(1):13–21
110. Zuluaga-Astudillo D, Ruge JC, Camacho-Tauta J, Reyes-Ortiz O, Caicedo-Hormaza B (2023) Diatomaceous soils and advances in geotechnical engineering—Part I. *Appl Sci* 13(1):549

Publisher's Note Springer Nature remains neutral with regard to jurisdictional claims in published maps and institutional affiliations.

Springer Nature or its licensor (e.g. a society or other partner) holds exclusive rights to this article under a publishing agreement with the author(s) or other rightsholder(s); author self-archiving of the accepted manuscript version of this article is solely governed by the terms of such publishing agreement and applicable law.